Co-published by
Institute of Fluid-Flow Machinery
Polish Academy of Sciences
Committee on Thermodynamics and Combustion
Polish Academy of Sciences

Copyright©2026 by the Authors under licence CC BY-NC-ND 4.0

http://www.imp.gda.pl/archives-of-thermodynamics/

Rheological and porous effects on mixed convection: Power-law fluid flow in a finned annular configuration

Youcef Lakahal*, Houssem Laidoudi

Faculty of Mechanical Engineering, University of Science and Technology of Oran Mohamed-Boudiaf, BP 1505, El -Menaouer, Bir El Djir 31000, Algeria
*Corresponding author email: youcef.lakahal@univ-usto.dz

Received: 07.06.2025; revised: 02.02.2026; accepted: 22.04.2026

Abstract

This study numerically investigates mixed-convection heat transfer of non-Newtonian power-law fluids in the annular space between a rotating outer cylinder and a stationary finned inner cylinder filled with a porous medium. The outer cylinder rotates at constant angular velocity and is maintained at a temperature lower than the finned inner cylinder, producing combined forced and buoyancy-driven flow. The governing equations were solved using the finite volume method implemented in Ansys CFX, with the fluid's rheology modelled by the Ostwald's law model. Parametric ranges include: Reynolds numbers from 5 to 35, Richardson numbers from 0 to 3, Darcy numbers from 10^{-5} to 10^{-2}, and power-law indices of 0.6, 1.0 and 1.6. The results show a transitional behaviour at a Richardson number of approximately 2.6 (for a Darcy number of 10^{-2}), beyond which the average Nusselt number becomes almost independent of the power-law index. Increasing rotational forcing enhances circulation and heat transfer, and under strong buoyancy the shear-thinning fluid (power-law index 0.6) yields up to 15–20% higher average heat transfer compared with the Newtonian case. The novelty of this work lies in the joint investigation of internal fins, outer-wall rotation and porous resistance in non-Newtonian media, which produces distinct flow regimes and offers practical guidance for porous heat exchanger and rotating-machine cooling designs.

Keywords: Complex fluid; Mixed convection; Porous media; Numerical investigation; Nusselt number; CFD

Vol. 47(2026), No. 3, 41–55; doi: 10.24425/ather.2026.3653

Cite this manuscript as: Lakahal, Y., & Laidoudi, H. (2026). Rheological and porous effects on mixed convection: Power-law fluid flow in a finned annular configuration. *Archives of Thermodynamics*, 47(3), 41–55.

1. Introduction

In recent years, the study of mixed convection in non-Newtonian or rheologically complex fluids has attracted considerable attention due to its importance in numerous engineering and industrial applications, including metal casting, enhanced oil recovery, glass manufacturing, biomedical devices and food processing. While many investigations have concentrated on forced convection in power-law fluids where flow is predominantly driven by external forces, researchers have also examined their thermal and flow behaviour around confined geometries, such as cylinders and ducts with different cross-sectional shapes. These studies often incorporate enclosures with adiabatic walls, structured inlets and outlets, or partially porous regions to better mimic real systems [1–3].

Complementary work has been devoted to natural convection, which arises solely from buoyancy forces induced by temperature gradients. Such investigations have considered power-law fluids within trapezoidal or wavy enclosures, typically featuring heated bases and either cooled or insulated boundaries [4,5].

Other studies have focused on rectangular and shallow cavities to evaluate how non-Newtonian rheology affects the onset of flow, velocity distribution, temperature fields and overall heat transfer efficiency under various thermal conditions [6,7].

Nomenclature

A – surface area of the inner cylinder, m^2
C_p – heat capacity of fluid, J/(kg K)
d – diameter of the inner cylinder, m
Gr – Grashof number
g – gravitational acceleration, m/s
I_2 – second invariant function of strain rate tensor
K – permeability, m^2
m – consistency index, Pa s^n
n – power-law index
Nu – Nusselt number (average value)
Nu_L – Nusselt number (local value)
p – pressure, Pa
Pr – Prandtl number
Re – Reynolds number
Ri – Richardson number
T – temperature, K
u, v – velocity components along x- and y-directions, m/s
x, y – Cartesian coordinates, m

Greek symbols

β_T – coefficient of volume expansion
η – dynamic viscosity, Pa s
ρ – density of fluid, kg/m^3
τ – stress tensor, Pa
Ω – rotation speed, 1/s

Subscripts and Superscripts

c – cold
h – hot
$*$ – dimensionless quantity

Abbreviations and Acronyms

ANN – artificial neural network
CFD – computational fluid dynamics

The interplay between forced and natural convection, known as mixed convection in power-law fluids, has also been widely analysed using numerical simulations. These studies emphasise the key influence of dimensionless parameters, such as the Reynolds number (Re), Richardson number (Ri) and power-law index (n) on both flow structures and heat transfer mechanisms. Investigations have been carried out in different geometries, including lid-driven and wall-driven cavities with isothermal, adiabatic or combined boundary conditions [8–13]. Configurations featuring internally heated blocks or asymmetric heating have revealed how geometric and thermal non-uniformities can modify flow circulation and enhance heat transfer [14–21].

Another aspect of growing interest is internal rotation within non-Newtonian domains. The presence of rotating components, such as cylinders, significantly affects streamlines, isotherms and the overall heat transfer rate, often characterised through the Nusselt number [22–27]. Further complexity has been introduced in studies involving triangular or inclined cavities filled with power-law nanofluids subjected to magnetic fields, where changes in parameters, such as Re, Ri, n and magnetic inclination, were found to strongly influence both heat and mass transport [28,29].

Recent numerical and experimental works have also explored complex geometries and non-uniform heating conditions, such as lid-driven cavities with embedded obstacles [30], compound cavity–channel systems incorporating multiple heat sources [31,32], and enclosures containing hemispherical heaters [33]. Investigations on micropolar and magnetised fluids have further demonstrated that localised magnetic effects can generate secondary vortices, enhancing flow mixing and thermal regulation [34]. Moreover, studies of double-lid cubic enclosures with distributed heat sources have highlighted the sensitivity of heat transfer and flow structures to variations in Re, Ri and nanoparticle concentration [35].

Recent developments in reliability engineering have emphasised the integration of machine learning with statistical modelling to improve predictive accuracy and system assessment. In [36,37], reliability analyses were conducted for the generalised exponential and generalised Rayleigh distributions, respectively, by incorporating the inverse power-law model within an artificial neural network (ANN) framework using Bayesian regularisation. These studies demonstrated that the combination of ANN-based learning and Bayesian regularisation significantly enhances the reliability prediction capability by minimising overfitting and improving model generalisation. The results confirmed that this hybrid approach provides more accurate lifetime estimation and better captures the complex reliability behaviour of engineering systems. Overall, [36,37] illustrate the growing potential of intelligent computational methods for advancing reliability modelling and analysis in modern industrial applications.

Despite this extensive literature, there remains a notable research gap concerning mixed convection in configurations that integrate rotating enclosures, internal fins and porous media. Most previous studies have addressed simpler geometries or neglected the presence of internal fins, even though fins play a vital role in modifying thermal performance by increasing the heat transfer surface area and disrupting flow symmetry. In addition, the effects of porous media on convective transport in non-Newtonian fluids have often been overlooked, limiting the practical relevance of existing models.

To address these gaps, the present study investigates mixed convection of power-law fluids in a complex annular configuration consisting of a rotating outer cylinder and a stationary finned inner cylinder embedded in a porous medium. This configuration is of particular interest for applications, such as rotating machinery, advanced cooling systems and compact heat exchangers. By systematically varying the Reynolds, Richardson, and Darcy numbers, as well as the power-law index, this work aims to clarify the coupled effects of rotation, non-Newtonian rheology, and porous resistance on fluid flow and heat transfer characteristics.

Numerical simulations are conducted using the finite volume method, providing detailed insights into the thermo-fluid dynamics within the enclosure. The results presented herein aim to

extend existing knowledge and offer a comprehensive framework for analysing non-Newtonian mixed convection in geometrically and physically complex systems relevant to modern thermal engineering applications.

2. Physical problem and mathematical formulations

Figure 1 presents the physical and computational configuration of the problem, consisting of a horizontal finned inner cylinder enclosed within a concentric outer cylinder. The inner cylinder, featuring uniformly distributed radial fins, is maintained at a higher temperature (T_h), while the outer boundary is held at a lower temperature (T_c), ensuring a consistent thermal gradient ($T_h > T_c$). The outer cylinder rotates counterclockwise with a constant angular velocity (Ω). The space between the two cylinders is filled with a porous medium saturated with a non-Newtonian power-law fluid. Three distinct power-law indices (n = 0.6, 1.0, and 1.6) are investigated to represent shear-thinning, Newtonian and shear-thickening behaviours, respectively.

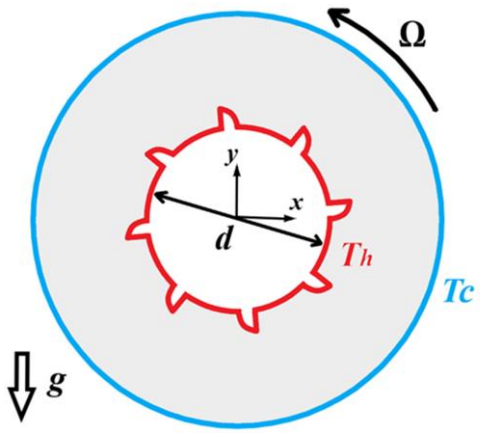


Fig. 1. Diagrammatic representation of the problem.

Mixed convection arises when both natural and forced convection mechanisms contribute to heat transfer. In this study, forced convection is induced by the rotation of the outer cylinder, while natural convection is driven by the temperature difference between the surfaces of the two cylinders. The Reynolds number determines the cylinder's rotational velocity value, while the Richardson number quantifies the balance between forced and natural convection effects. Four Richardson numbers are analysed: 0, 1, 2 and 3. The medium's permeability, represented by the Darcy number (Da), is investigated within the range of 10^{-5} to 10^{-2}.

The assumptions of laminar and non-Newtonian flow, steady state, mixed convection and constant fluid properties are adopted in this study. The equations of continuity, momentum and energy, subject to the Boussinesq approximation and the effect of negligible dissipation, are written in their dimensionless form as follows:

– the equation of continuity:

$$\frac{\partial u^*}{\partial x^*} + \frac{\partial v^*}{\partial y^*} = 0, \tag{1}$$

– the equation of momentum along the x-direction:

$$u^*\left(\frac{\partial u^*}{\partial x^*}\right) + v^*\left(\frac{\partial v^*}{\partial y^*}\right) = -\frac{\partial p^*}{\partial x^*} + \frac{1}{\mathrm{Re}}\left(\frac{\partial \tau^*_{xx}}{\partial x^*} + \frac{\partial \tau^*_{yx}}{\partial y^*}\right), \tag{2}$$

– the equation of momentum along the y-direction:

$$u^*\left(\frac{\partial v^*}{\partial x^*}\right) + v^*\left(\frac{\partial v^*}{\partial y^*}\right) = -\frac{\partial p^*}{\partial y^*} + \frac{1}{\mathrm{Re}}\left(\frac{\partial \tau^*_{xy}}{\partial x^*} + \frac{\partial \tau^*_{yy}}{\partial y^*}\right) + \mathrm{Ri}\, T^*, \tag{3}$$

– the equation of energy:

$$u^*\left(\frac{\partial T^*}{\partial x^*}\right) + v^*\left(\frac{\partial T^*}{\partial y^*}\right) = \frac{1}{\mathrm{Pe}}\left(\frac{\partial^2 T^*}{\partial x^{*2}} + \frac{\partial^2 T^*}{\partial y^{*2}}\right), \tag{4}$$

where Re and Pe are the Reynolds and Peclet numbers, Ri is the Richardson number, u^* and v^* are the fluid dimensionless velocities in the x^*- and y^*-directions, and dimensionless pressure and temperature are represented by p^* and T^*, respectively. The following represent the dimensionless variables:

$$x^* = \frac{x}{d}, \quad y^* = \frac{y}{d}, \tag{5}$$

$$u^* = \frac{u}{\Omega d}, \quad v^* = \frac{v}{\Omega d}, \tag{6}$$

$$p^* = \frac{p}{\rho(\Omega d)^2}, \quad T^* = \frac{T - T_c}{T_h - T_c}, \tag{7}$$

$$\mathrm{Pe} = \mathrm{RePr}. \tag{8}$$

where Pr is the Prandtl number and d is the inner cylinder's diameter.

The following equation represents the power-law fluid's behaviour:

$$\tau_{ij} = 2\eta\varepsilon_{ij}, \tag{9}$$

where the viscous stress tensors and the rate of deformation are represented, respectively, by ε_{ij} and τ_{ij}. ($i, j = x, y$). Furthermore, for power-law fluids, the fluid viscosity, denoted by η, is defined (in dimensional form) as follows:

$$\eta = m\left(\frac{I_2}{2}\right)^{\left(\frac{n-1}{2}\right)}, \tag{10}$$

where I_2 is the second invariant of the rate of deformation tensor, m is the consistency index, and n is the power-law index. A fluid that is shear-thinning is represented by $n < 1$, a Newtonian limit by a value of $n = 1$, and a shear-thickening fluid by $n > 1$. The following equation gives I_2 in Cartesian coordinates:

$$\left(\frac{I_2}{2}\right) = 2\left(\frac{\partial u}{\partial x}\right)^2 + 2\left(\frac{\partial v}{\partial y}\right)^2 + \left[\left(\frac{\partial u}{\partial y}\right) + \left(\frac{\partial v}{\partial x}\right)\right]^2. \tag{11}$$

Generally, Grashof number, Richardson number and Darcy number for power-law fluids are computed as follows:

$$\mathrm{Gr} = g\beta_T \Delta T d^3 \left(\frac{\rho}{m}\Omega^{1-n}\right)^2, \tag{12}$$

$$\mathrm{Ri} = \frac{g\beta_T \Delta T d^3}{(\Omega d)^2} = \frac{\mathrm{Gr}}{\mathrm{Re}^2}, \tag{13}$$

$$\mathrm{Da} = \frac{K}{d^2}, \tag{14}$$

where ρ, g, β_T, and K are the density of the fluid, the gravitational acceleration, volumetric expansion coefficient and permeability, respectively.

The Nusselt number, or average Nusselt number, is calculated by integrating local values along the inner cylinder's surface. The following are the local and average values of Nu, respectively:

$$\mathrm{Nu}_L = \left(\frac{\partial T^*}{\partial n}\right)_{wall}, \quad \mathrm{Nu} = \frac{1}{A}\int_S \mathrm{Nu}_L dA, \tag{15}$$

where $\boldsymbol{n}$ is the normal vector to the wall and S represents the surface of the heated inner cylinder.

3. Numerical procedure

The numerical simulations in this study were carried out using Ansys-CFX, a commercial computational fluid dynamics (CFD) tool that transforms the governing equations of fluid flow and heat transfer into algebraic form. These equations were discretised using the finite volume method, with boundary conditions applied throughout the computational domain. To ensure high solution accuracy, a convergence criterion of 10^{-6} was adopted for both the momentum and energy equations. The high-resolution scheme was utilised to accurately capture convection effects, while the SIMPLEC (semi-implicit method for pressure linked equations-consistent) algorithm was implemented to efficiently couple pressure and velocity fields, offering enhanced stability for steady-state analyses.

To validate the accuracy of the numerical results, a grid independence study was conducted, acknowledging the significant influence of mesh resolution on simulation precision. The computational domain was discretised using a hybrid mesh structure with refined quadrilateral elements in the vicinity of the inner and outer walls to better resolve boundary layer gradients. As illustrated in Fig. 2 and detailed in Table 1, three progressively refined mesh configurations were examined: M1 (coarse), M2 (medium) and M3 (fine). The average Nusselt number along the heated cylindrical surface was calculated

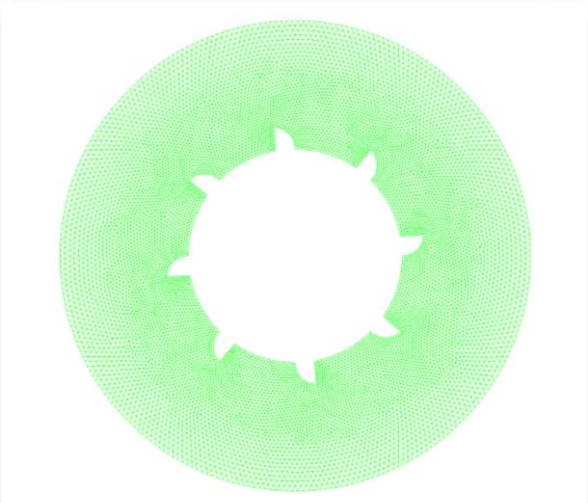


Fig. 2. The structure of the grid used for the calculations.

Table 1. Grid independency test for n = 1.6, Re = 25, Ri = 3 and Da = 10^{-3}.

Mesh	Elements	Nusselt number	Difference, %
M1	122 000	1.50581	1.53
M2	244 000	1.48278	0.0112
M3	488 000	1.48294	–

under representative conditions: n = 1.6, Re = 25, Ri = 3 and Da = 10^{-3}. The comparison showed that the medium-resolution mesh (M2) produced results nearly identical to those of the finest mesh (M3), confirming that M2 offers an optimal compromise between computational efficiency and solution accuracy. Hence, M2 was selected for all subsequent simulations, balancing computational cost and numerical precision.

The accuracy and robustness of the present numerical model were verified through comparisons with established benchmark studies. The first validation involved comparing results with the classical work of Kuehn and Goldstein [38] and the study by Matin and Khan [39], both of which examined buoyancy-driven flow in annular enclosures. For this case, the working fluid was considered Newtonian (n = 1) with properties of air (Pr = 0.71), and the Rayleigh number was varied from 10^3 to 10^6. As shown in Fig. 3A, the predicted variation of the average Nusselt number with Rayleigh number (Ra = Pr Gr) for Pr = 0.71 and n = 1 closely matches the reference data, confirming the model's ability to capture natural convection phenomena accurately.

A second comparison assessed the model's capability to represent non-Newtonian fluid behaviour, focusing on the influence of the power-law index. Results were compared to those reported by Matin et al. [40] under conditions of Pr = 100 and a blockage ratio of 0.25. The present model reproduced the same trend of heat transfer enhancement for shear-thinning fluids (n < 1) and suppression for shear-thickening fluids (n > 1), consistent with theoretical expectations. Figure 3B illustrates strong agreement in the Nusselt number variation with respect to n, validating the model's treatment of fluid rheology and ensuring accurate representation of non-linear viscosity effects.

Lastly, validation was extended to the study by Sheikholeslami [41], which investigated natural convection between concentric cylinders filled with a porous medium and subjected to a temperature difference between the inner and outer walls. The comparison was made at Da = 10^{-3} and Ra = 10^5. As seen in Fig. 3C, the present results show excellent consistency with the benchmark, further supporting the reliability of the adopted numerical approach. The close match across multiple validation cases confirms that the current CFD model is robust and capable of accurately resolving complex coupled effects of buoyancy, rotation and non-Newtonian fluid rheology in porous media.

4. Results and discussion

This study investigates the heat transfer and flow behaviour of a power-law fluid in a porous medium confined between a stationary finned inner cylinder and a rotating outer cylinder. The analysis focuses on the influence of key parameters: the Reynolds number (Re = 5, 15, 25 and 35), Richardson number (Ri = 0, 1, 2

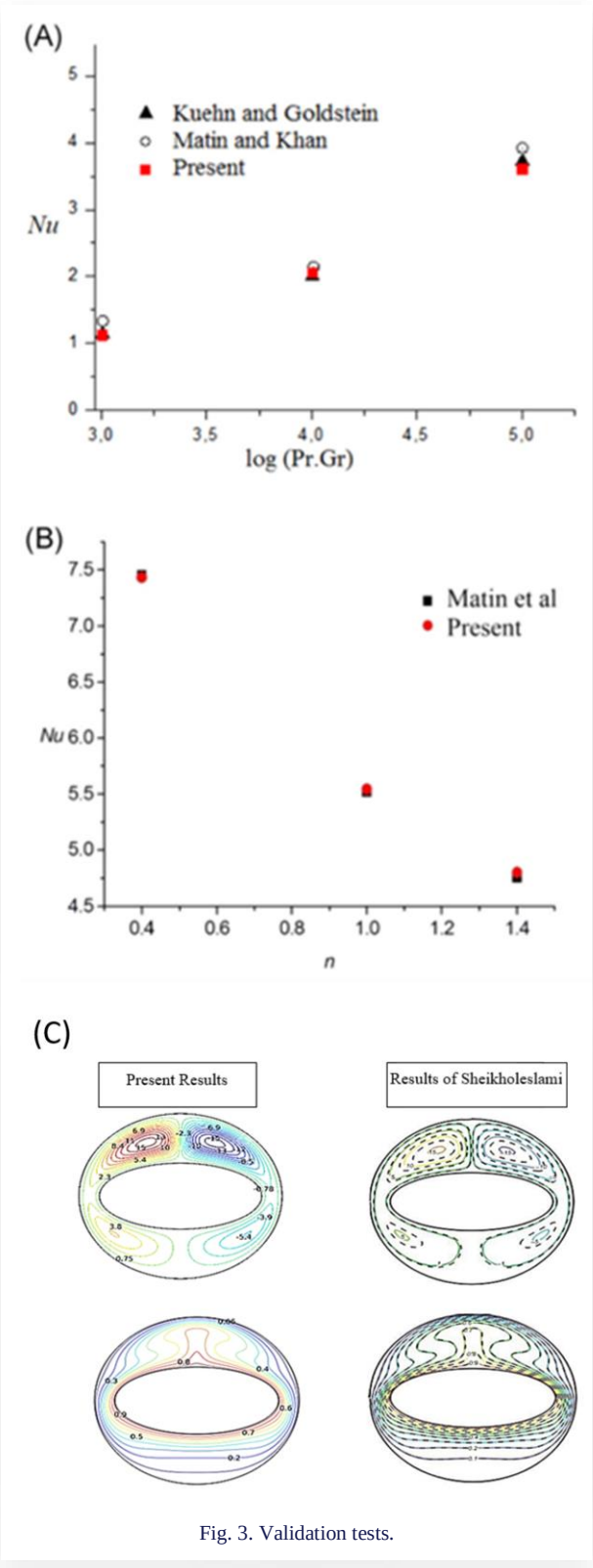


Fig. 3. Validation tests.

and 3), Darcy number (Da = 10^{-5} to 10^{-2}) and power-law index (n = 0.6, 1 and 1.6), with a fixed Prandtl number (Pr = 50). Flow dynamics and thermal performance are explored using streamlines, isotherms and the Nusselt number. Some parameter values are selected based on a previous study [42].

Mixed convection arises when both forced and natural convection mechanisms coexist. In this study, natural convection is driven by the temperature difference between the two cylinders, while forced convection results from the rotation of the outer cylinder. When Ri = 0, the flow is purely governed by forced convection. As Ri increases, buoyancy forces (representing natural convection) gradually become more significant. Simultaneously, the rotational speed of the outer cylinder, which governs the magnitude of forced convection, increases with Reynolds number.

Figure 4 illustrates the flow patterns represented by streamlines for various Reynolds numbers and power-law indices. At low Re, viscous forces dominate, resulting in smooth, symmetric streamlines around the finned inner cylinder. The flow remains relatively weak, with minimal recirculation. As Re increases, inertial effects become more pronounced, leading to the formation of a closed counter-rotating vortex on the left side of the domain. The streamlines extend further outward and form larger vortices, reflecting intensified flow activity around the fins.

At higher Re, the centrifugal force generated by the rotating outer cylinder significantly enhances momentum transfer, resulting in asymmetric vortical structures that extend toward the upper region of the enclosure. The secondary vortices near the fin tips indicate localised shear-layer separations, which enhance local mixing and amplify heat exchange along the finned surfaces.

For shear-thinning fluids (n = 0.6), the apparent viscosity decreases with increasing shear rate, which enhances fluid motion and results in more elongated and active recirculation zones, especially at higher Re. In contrast, as the power-law index increases (n = 1.6, shear-thickening behaviour), viscosity increases with shear rate, damping the fluid motion. This suppresses vortex formation, leading to smaller and less intense recirculation zones compared to the shear-thinning case.

Figure 5 displays the thermal fields (isotherms) under the same parameter conditions. The temperature distribution closely mirrors the fluid flow patterns. At low Re, nearly concentric isotherms are observed around the heated inner cylinder, indicating weak convective effects and localised thermal gradients. As Re increases, convection dominates, distorting the isotherms and pushing them outward due to intensified fluid motion.

This outward displacement signifies a transition from conduction-controlled to convection-dominated transport. The stretching of isotherms in the direction of rotation reflects enhanced azimuthal heat transport, while compression near stagnation zones reveals localised temperature build-up due to limited mixing.

The rotational direction of the outer cylinder enhances the effect of buoyancy on the right side of the domain, promoting heat transfer. On the upper part of the inner cylinder, the isotherms are further stretched and distorted, indicating stronger convective mixing. On the left side, however, the presence of recirculating flow thickens the isotherms and reduces thermal transport efficiency. A more detailed observation shows that the region downstream of the fin tip experiences a local thermal wake, where thermal diffusion dominates due to reduced local velocity magnitude. A notable feature is the tongue-like structure in the thermal boundary layer at the top of the inner cylinder. This structure reflects reduced fluid mixing, which limits

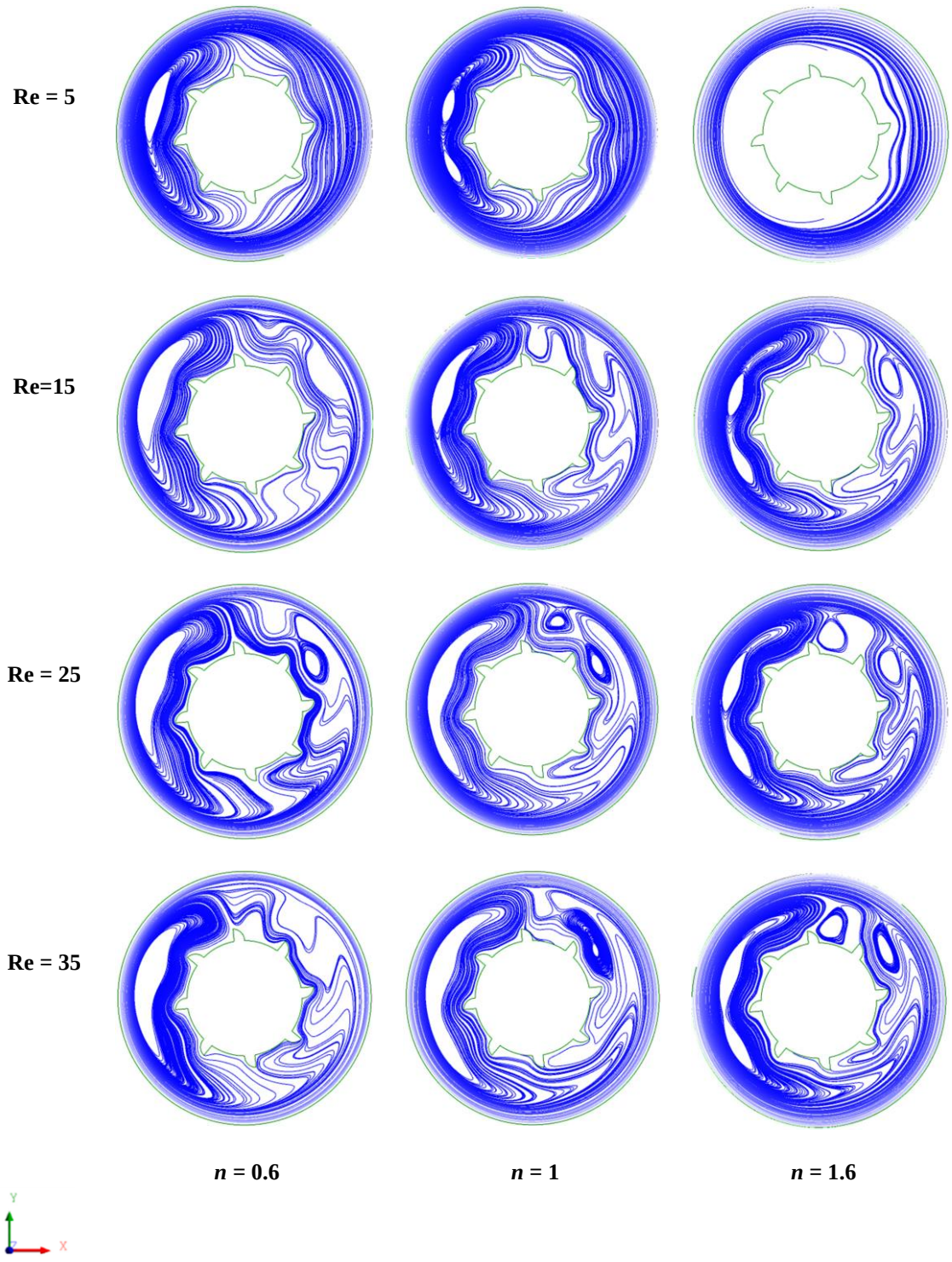


Fig. 4. Streamlines for various values of Re and n at Da = 10^{-2} and Ri = 3.

convective heat dispersion. As n increases, this tongue splits into two branches due to altered flow patterns. This bifurcation represents a competition between viscous damping (which stabilises the thermal layer) and centrifugal enhancement (which destabilises it). The higher viscosity of shear-thickening fluids suppresses upward motion above the finned cylinder, leading to localised heat accumulation and bifurcated thermal zones around the fins.

Figure 6 illustrates the flow patterns represented by streamlines for various Richardson numbers and power-law indices, at fixed values of Reynolds number (Re = 25) and Darcy number (Da = 10^{-2}). When Ri is low, forced convection is dominant, resulting in a stable rotational flow between the cylinders. As Ri increases, buoyancy forces become more significant, giving rise to vertically oriented flow structures and the development of counter-rotating vortices. At intermediate Ri (= 1–2), the flow field exhibits mixed characteristics; the

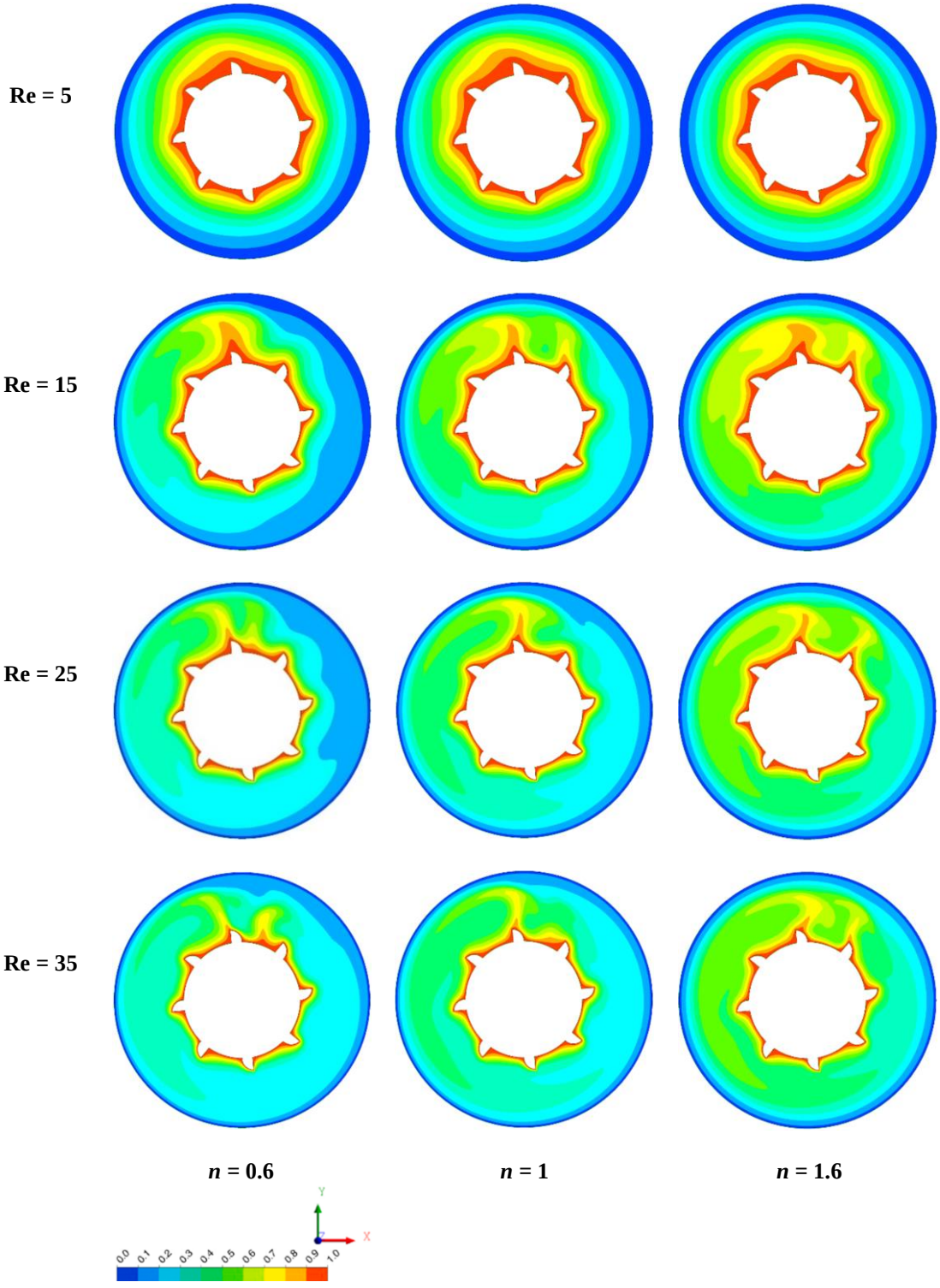


Fig. 5. Isotherms for various values of Re and n at Da = 10^{-2} and Ri = 3.

upper vortex strengthens as buoyancy lifts hot fluid upward, while the lower region remains rotation-driven. This dual mechanism introduces asymmetry in the streamline topology, redistributing shear stresses along the finned surface.

For the shear-thinning fluid (n = 0.6), the enhanced flow mobility leads to more elongated and active recirculation zones. In contrast, increasing n suppresses these features: the shear-thickening fluid (n = 1.6) exhibits higher apparent viscosity, which dampens the flow and yields smaller, weaker vortices. This demonstrates that buoyancy–viscosity coupling is nonlinear: buoyancy-induced motion is amplified in low-viscosity regions (shear-thinning), but strongly suppressed in high-viscosity zones (shear-thickening), leading to distinct thermal stratifications.

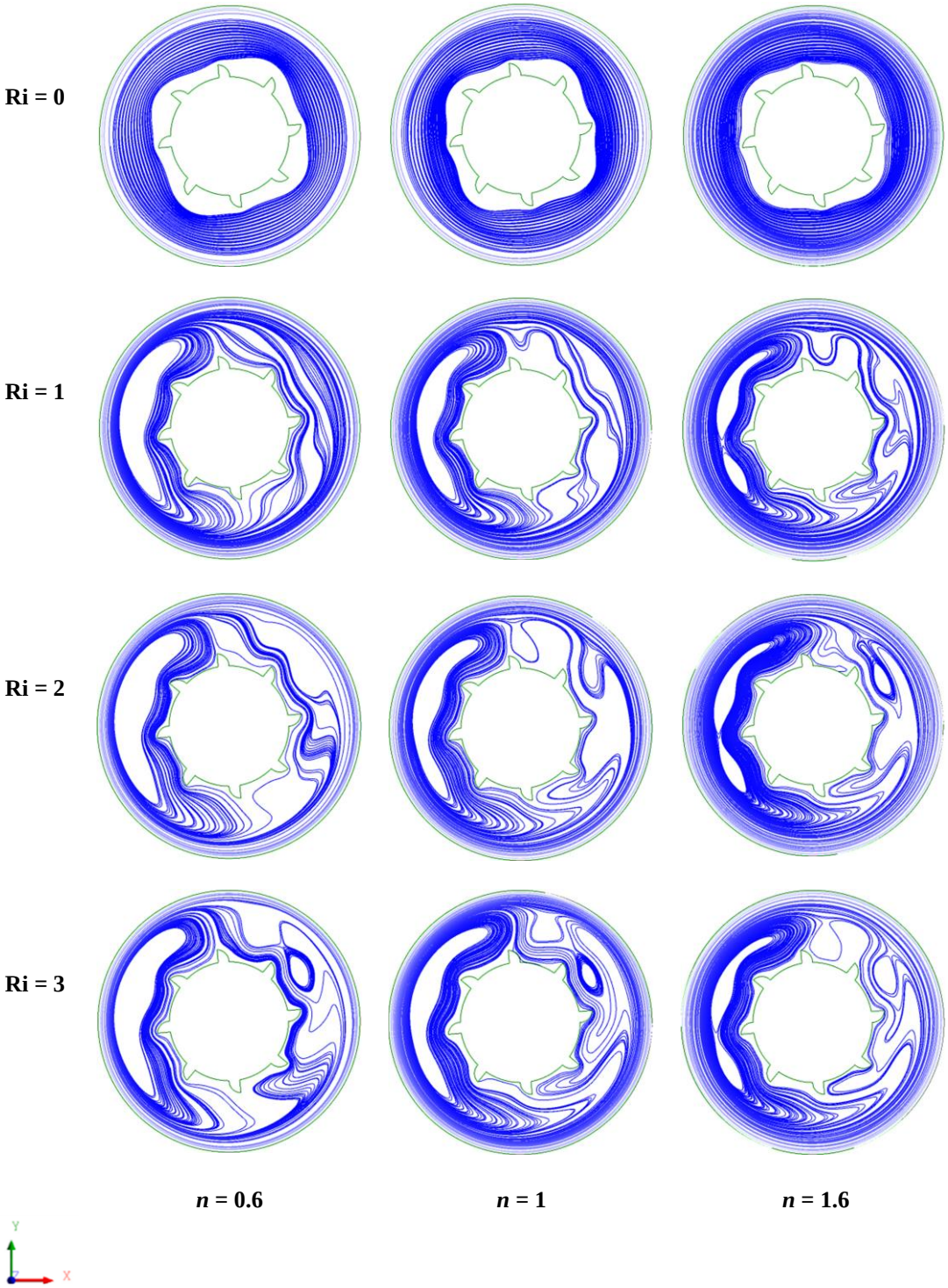


Fig. 6. Streamlines for various values of Ri and *n* at Da = 10^{-2} and Re = 25.

Figure 7 presents the corresponding isotherms under the same conditions. At Ri = 0, the isotherms remain nearly parallel, showing that forced convection dominates. As Ri increases, the isotherms distort vertically, indicating a growing influence of buoyancy-driven flow. The upward migration of isotherms at higher Ri indicates the formation of a thermal plume above the inner cylinder, characteristic of buoyancy-dominated convection. The left–right asymmetry intensifies with Ri increase, showing that buoyancy breaks rotational symmetry and creates preferential heat pathways along the upward direction.

For n = 0.6, the higher mobility produces thinner thermal boundary layers and more dispersed temperature fields. In contrast, for n = 1.6, reduced motion thickens the thermal layers, limiting heat diffusion and causing localised heat build-up near the inner cylinder. This inverse relationship between viscosity

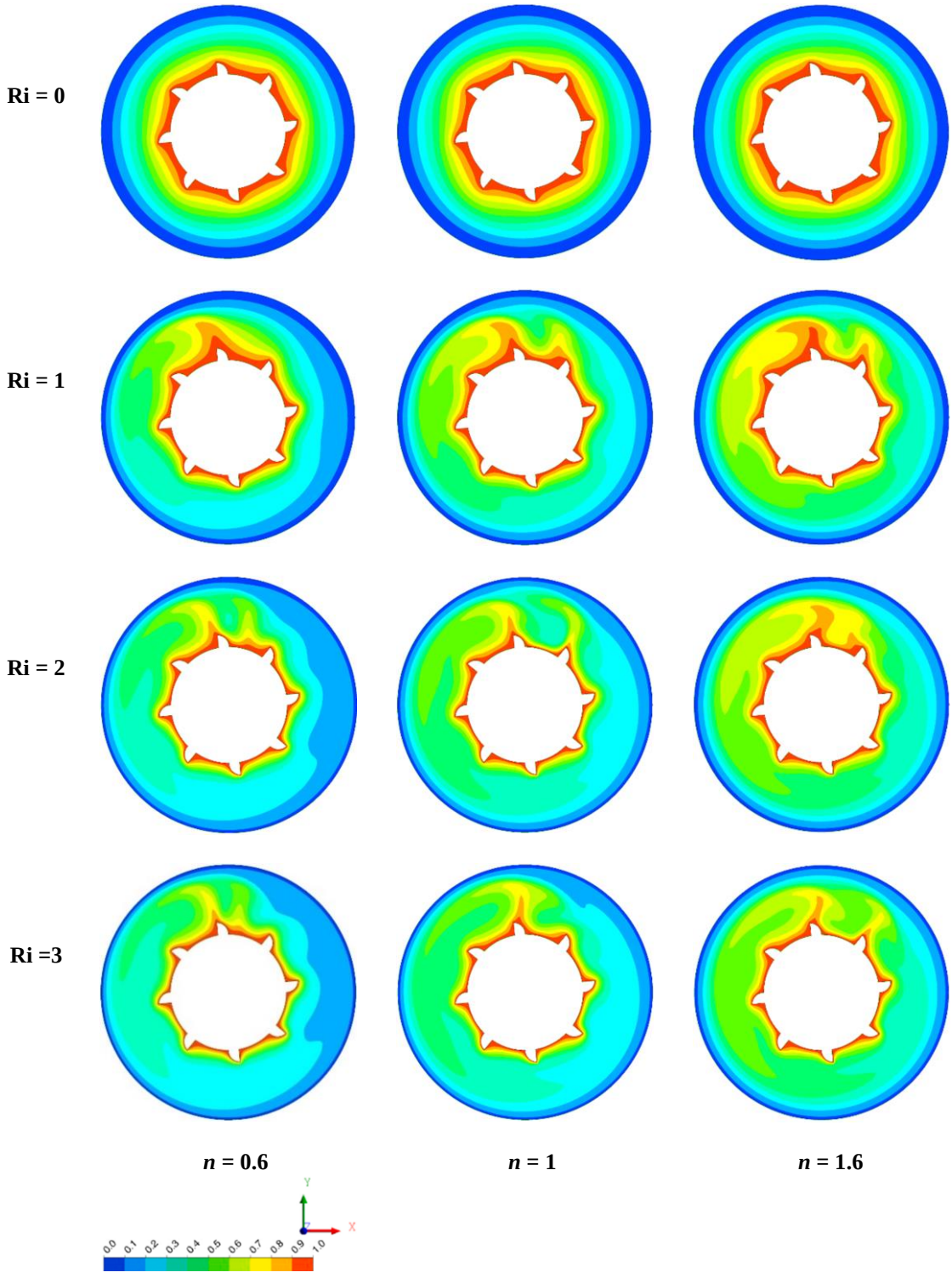


Fig. 7. Isotherms for various values of Ri and n at Da = 10^{-2} and Re = 25.

and boundary-layer thickness confirms that rheological properties govern not only momentum diffusion, but also the thermal resistance adjacent to the heated surfaces.

Figure 8 shows the streamline patterns for various Darcy numbers and power-law indices, at fixed Re = 25 and Ri = 3. At low Da, the porous matrix restricts fluid motion, resulting in weak, localised recirculation around the finned cylinder. As Da increases, permeability improves, allowing stronger motion and larger vortices to form. At intermediate Da values (10^{-4}–10^{-3}), the competition between viscous drag and porous resistance yields a partially developed circulation where flow leakage through the porous matrix modifies vortex symmetry. This interplay introduces a mixed conduction–convection regime that is highly sensitive to n.

For n = 0.6, shear-thinning behaviour intensifies recirculation, especially at higher Da, while for n = 1.6, higher viscosity inhibits

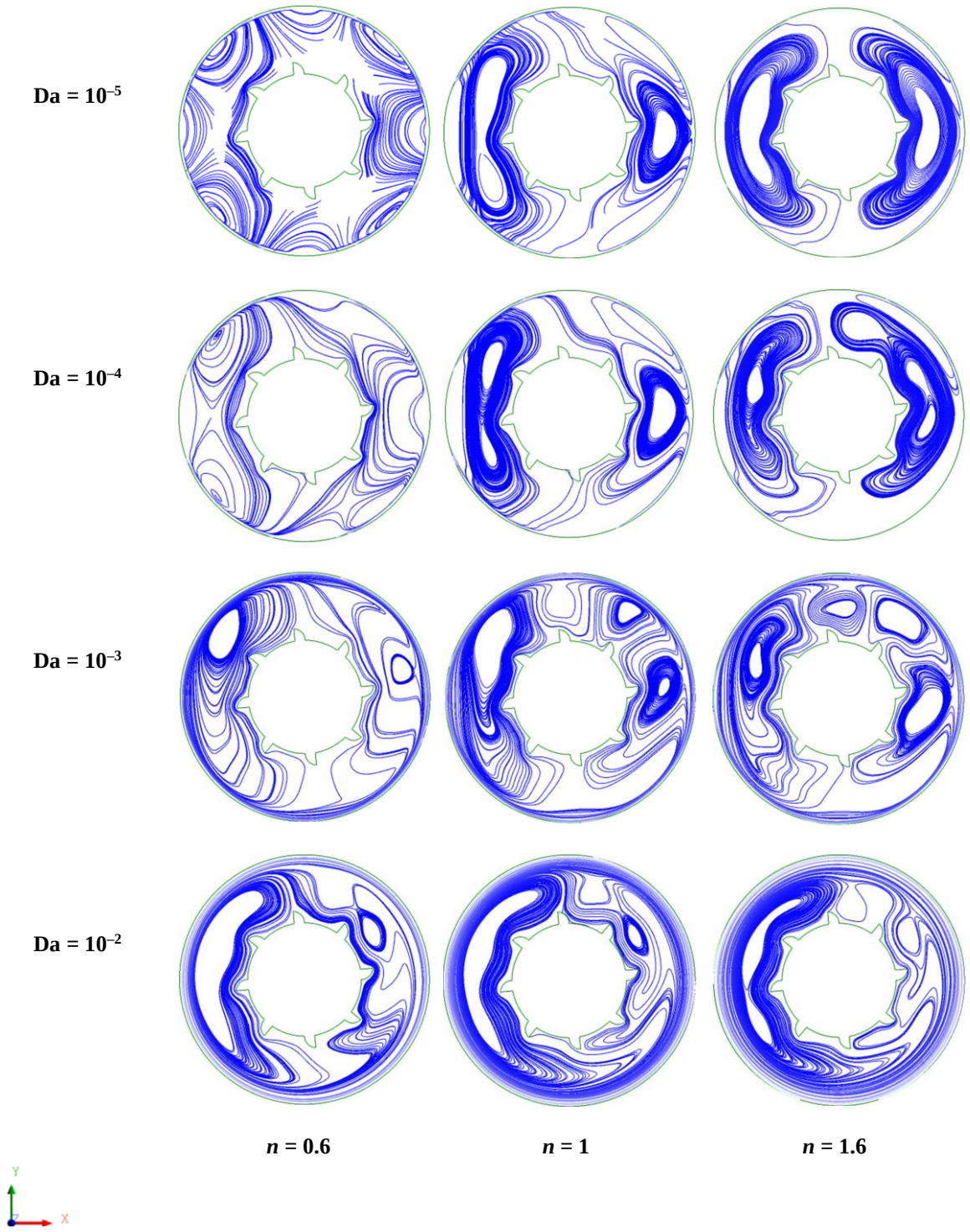


Fig. 8. Streamlines for various values of Da and *n* at Re = 25 and Ri = 3.

vortex development, producing smaller and weaker zones. This behaviour underscores that the porous structure modulates the influence of non-Newtonian viscosity; permeability enhancement magnifies rheological effects, whereas low Da dampens them.

Figure 9 displays the associated isotherms for the same Da, Re and Ri conditions. At low Da, limited flow mobility yields nearly concentric isotherms, reflecting conduction-dominated heat transfer. As Da increases, enhanced convection stretches and distorts the isotherms outward, especially for $n = 0.6$, which exhibits thinner boundary layers and better heat dispersion. The deformation of isotherms indicates a transition from localised conduction to bulk convection. At high Da, the temperature contours align with the dominant flow direction, confirming that fluid advection becomes the main heat transport mechanism.

For $n = 1.6$, high viscosity reduces fluid motion, producing thicker isotherms and localised thermal accumulation near the heated surface. These results emphasise the complex interaction between fluid rheology and porous-medium permeability in

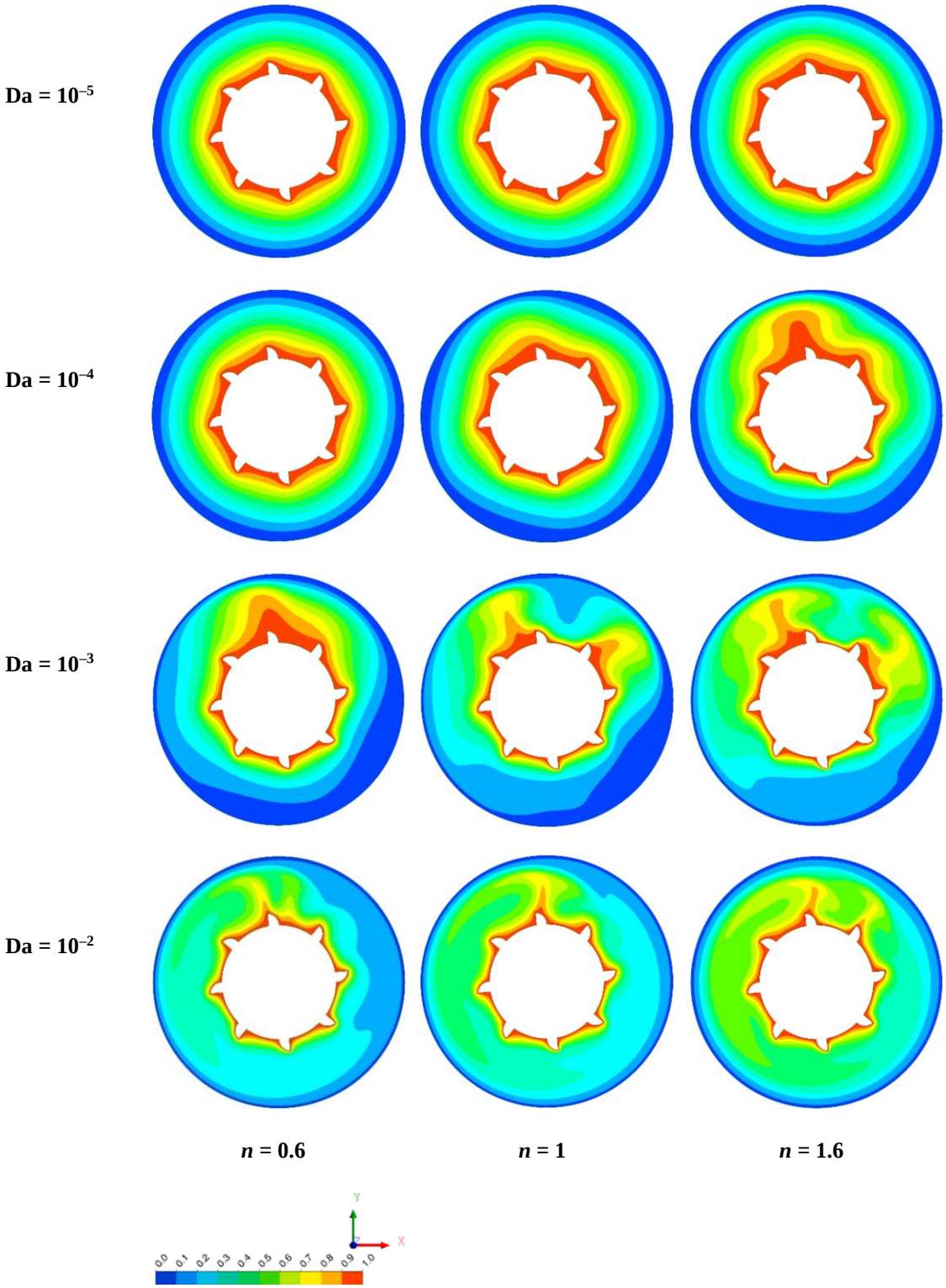


Fig. 9. Isotherms for various values of Da and *n* at Re = 25 and Ri = 3.

governing thermal transport. From a design standpoint, increasing Da enhances heat transfer up to a threshold, beyond which excessive permeability may shorten fluid residence time and slightly diminish local heat exchange.

Figure 10 illustrates how the average Nusselt number varies with Richardson number, power-law index and Reynolds number, at a fixed Darcy number ($Da = 10^{-2}$). At Re = 5, Nu remains nearly constant across Ri values, indicating that viscous effects dominate and suppress convective mixing. In this low-Re regime, heat transfer occurs mainly through conduction-like mechanisms, with negligible contributions from buoyancy forces.

As Re increases to 15 and 25, Nu rises more noticeably with Ri, reflecting the strengthening interaction between forced and natural convection. In these regimes, forced convection provides the baseline flow, while buoyancy-driven motion enhances mixing and promotes more effective thermal transport. The highest

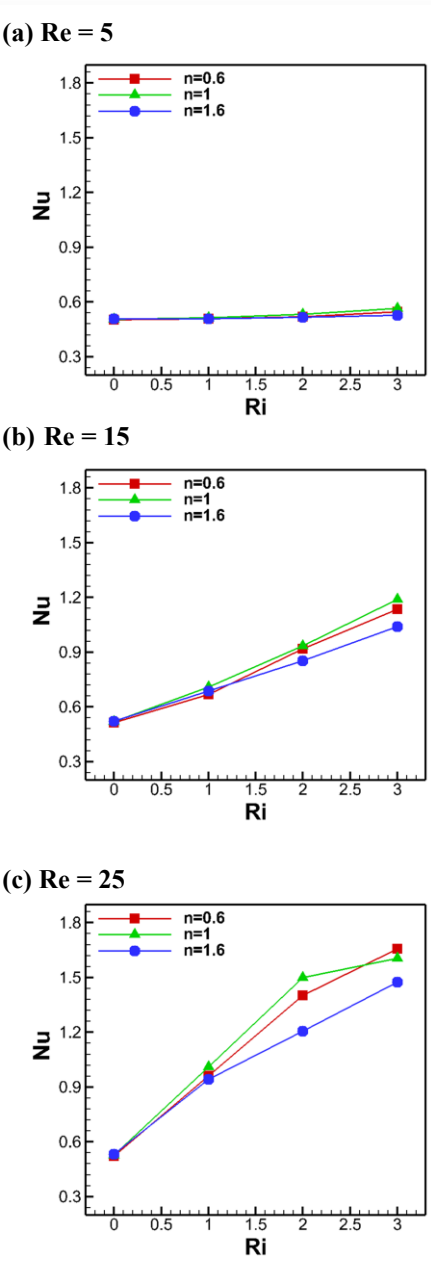


Fig. 10. Values of Nu vs. Ri and n at Da = 10^{-2} for: (a) Re = 5, (b) Re = 15 and (c) Re = 25.

Nu values are typically observed for n = 1 (Newtonian fluid), which balances fluid mobility and thermal diffusion most effectively.

For n = 0.6 (shear-thinning fluid), Nu values are generally lower than those for Newtonian fluids under most conditions, particularly at lower Re or Ri. Although reduced viscosity promotes flow mobility, it may reduce thermal gradients and limit effective mixing. However, at higher Re and Ri (where inertial and buoyancy effects dominate) this enhanced mobility can improve thermal performance. For example, at Re = 25 and Ri = 3, Nu for n = 0.6 surpasses that of n = 1. On the other hand, for n = 1.6 (shear-thickening fluid), increased viscosity restricts motion and leads to the lowest Nu values across all conditions examined.

Figure 11 presents the variation of Nu with Ri, n and Da, at fixed Re = 25. The influence of Da is strongly dependent on fluid rheology, indicating nonlinear interactions between permeability, viscosity behaviour and thermal gradients. At Da = 10^{-5}, the porous medium resists flow significantly, resulting in conduction-dominated heat transfer, where Nu remains low and nearly constant across all values of n and Ri. As Da increases to 10^{-4}

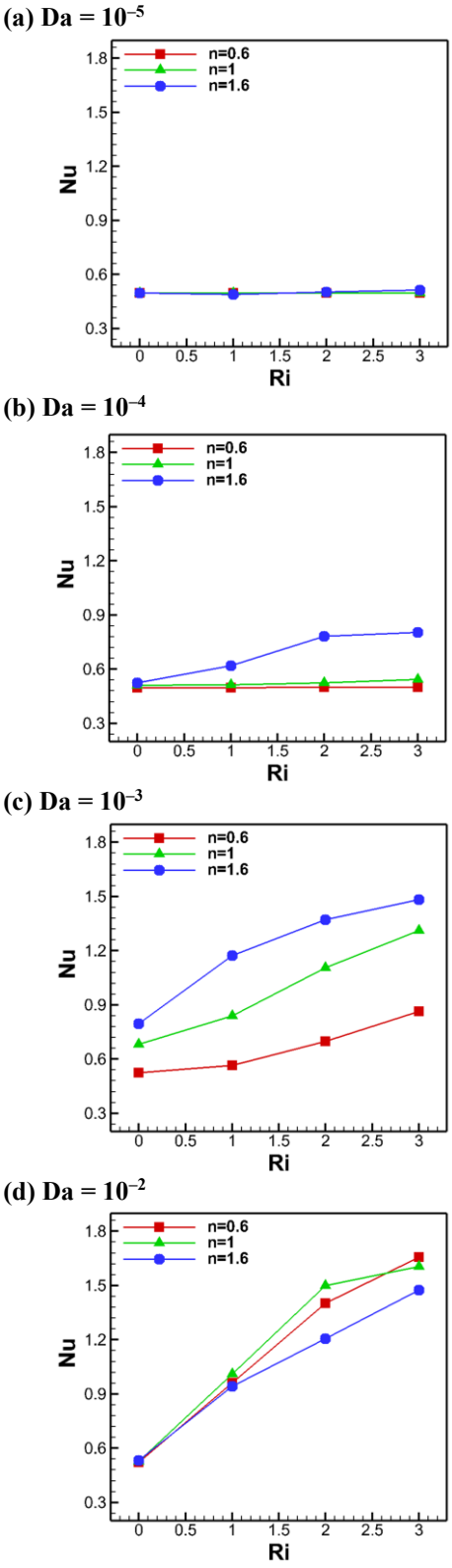


Fig. 11. Values of Nu vs. Ri and n at Re = 25 for: (a) Da = 10^{-5}, (b Da = 10^{-4}, (c) Da = 10^{-3} and (d) Da = 10^{-2}.

and 10^{-3}, permeability improves, allowing more vigorous convection and higher Nu values. Interestingly, the highest Nu values at these intermediate Da levels are observed for $n = 1.6$ (shear-thickening fluid). This suggests that, under moderate resistance, the increased shear-dependent viscosity promotes stronger temperature gradients and localised heat transfer enhancement.

At Da = 10^{-2}, the porous medium offers minimal resistance to flow, leading to robust convective heat transfer. Under these conditions, Newtonian fluids ($n = 1$) exhibit the highest Nu, benefiting from an optimal trade-off between flow and heat dispersion. Shear-thickening fluids ($n = 1.6$) underperform in this regime due to their higher viscosity, which limits motion and thermal mixing. Although shear-thinning fluids ($n = 0.6$) benefit from enhanced flow mobility, they do not achieve the highest Nu under any condition shown. This indicates that, despite faster flow, their reduced viscosity may hinder the development of strong thermal gradients, which are essential for efficient heat transfer.

A particularly noteworthy observation in Fig. 11 (for Da = 10^{-2}) is the critical Richardson number around Ri = 2.6, where the Nu values for the shear-thinning fluid ($n = 0.6$) and the Newtonian fluid ($n = 1$) intersect. This intersection marks a shift in the dominant heat transfer mechanism. For Ri < 2.6, Newtonian fluids outperform due to their balanced viscosity, which supports both momentum and thermal diffusion in mixed convection. As Ri increases and buoyancy dominates, the low viscosity of shear-thinning fluid allows for stronger buoyancy-driven flows and more effective convective mixing. Beyond Ri = 2.6, Nu for $n = 0.6$ exceeds that for $n = 1$, indicating better thermal performance in natural convection regimes. This finding highlights the nonlinear interaction between rheological properties and buoyancy forces, with important implications for optimising thermal systems involving non-Newtonian fluids in porous enclosures.

5. Conclusions

This study presented a numerical investigation of mixed convection heat transfer in a porous annulus formed by a stationary finned inner cylinder and a rotating outer cylinder, filled with a non-Newtonian power-law fluid. The governing equations were solved using the finite-volume method implemented in Ansys-CFX, with the fluid's rheology represented by the Ostwald's law model. The analysis systematically examined the combined influence of four key dimensionless parameters − the Reynolds number (Re), the Richardson number (Ri), the power-law index (n) and the Darcy number (Da) − on flow behaviour and heat transfer performance. The main conclusions are summarised as follows:

1) Increasing the Reynolds number from 5 to 25 enhances the flow circulation and convective strength, leading to a nearly 300% rise in the average Nusselt number at Ri = 3.
2) Shear-thinning fluids promote more vigorous recirculation and outperform Newtonian fluids ($n = 1.0$) under buoyancy-dominated conditions (Ri ≥ 2), while shear-thickening fluids ($n = 1.6$) suppress motion and reduce thermal transport due to their elevated apparent viscosity.
3) A transitional Richardson number of about Ri = 2.6 (for Da = 10^{-2}) marks the point where the Nusselt number becomes nearly independent of the power-law index. Beyond this value, shear-thinning fluids achieve 15–20% higher heat transfer than Newtonian fluids due to stronger buoyancy-driven circulation.
4) Porous permeability (Da) strongly affects the convection regime. Low Da values produce conduction-dominated flow, while higher Da ($\geq 10^{-3}$) enhances convective mixing and results in substantially larger Nusselt numbers through the combined effect of rotation and buoyancy.
5) Flow and thermal structures demonstrate nonlinear coupling among rheology, porous resistance and rotation, which controls the balance between forced and natural convection and defines the system's overall heat transfer efficiency.

These findings provide practical design insights for engineers developing compact thermal systems, including porous heat exchangers, geothermal units and rotating machinery cooling devices. The results enable the optimised selection of working fluids and operating parameters to achieve efficient performance under different flow and thermal conditions. Moreover, the integration of machine learning and optimisation techniques offers promising opportunities for the next generation of energy and cooling systems, particularly in applications where the interaction between non-Newtonian fluids and porous media plays a crucial role in determining system efficiency and reliability.

References

[1] Helmaoui, M., Laidoudi, H., Belbachir, A., Ayad, A., & Ghaniam, A. (2020). Forced convection heat transfer from a pair of circular cylinders confined in ventilated enclosure. *Diffusion Foundations*, 26, 104–111. doi: 10.4028/www.scientific.net/DF.26.104

[2] Mishra, L., Baranwal, A., & Chhabra, R. (2017). Laminar forced convection in power-law fluids from two heated cylinders in a square duct. *International Journal of Heat and Mass Transfer*, 113, 589–612. doi: 10.1016/j.ijheatmasstransfer.2017.05.117

[3] Mohebbi, R., Delouei, A.A., Jamali, A., Izadi, M., & Mohamad, A.A. (2019). Pore-scale simulation of non-Newtonian power-law fluid flow and forced convection in partially porous media: Thermal lattice Boltzmann method. *Physica A*, 525, 642–656. doi: 10.1016/j.physa.2019.03.039

[4] Malkeson, S.P., Alshaaili, S., & Chakraborty, N. (2023). Numerical investigation of steady state laminar natural convection of power-law fluids in side-cooled trapezoidal enclosures heated from the bottom. *Numerical Heat Transfer, Part A: Applications*, 83(7), 770–789. doi: 10.1080/10407782.2022.2157353

[5] Rashid, U., Shahzad, H., Lu, D., Wang, X., & Majeed, A.H. (2023). Non-Newtonian MHD double diffusive natural convection flow and heat transfer in a crown enclosure. *Case Studies in Thermal Engineering*, 41, 102541. doi: 10.1016/j.csite.2022.102541

[6] Lamsaadi, M., Naïmi, M., & Hasnaoui, M. (2005). Natural convection of non-Newtonian power law fluids in a shallow horizontal rectangular cavity uniformly heated from below. *Heat and Mass Transfer*, 41, 239–249. doi: 10.1007/s00231-004-0530-8

[7] Lamsaadi, M., Naïmi, M., Hasnaoui, M., & Mamou, M. (2006). Natural convection in a vertical rectangular cavity filled with a non-Newtonian power-law fluid and subjected to a horizontal temperature gradient. *Numerical Heat Transfer, Part A*, 49(10), 969–990. doi: 10.1080/10407780500324988

[8] Mahmood, F.T, Chowdhury, T.S., & Hasan, M.N. (2024). Fluid-structure interaction induced mixed convection characteristics in a lid-driven square cavity with non-Newtonian power-law fluids. *International Journal of Thermofluids*, 22, 100687. doi: 10.1016/ j.ijft.2024.100687

[9] Bilal, S., Khan, N.Z., Fatima, I., Riaz, A., Ansari, G.J., Alhazmi, S.E., & Tag El-Din, E.M. (2022). Mixed convective heat transfer in a power-law fluid in a square enclosure: Higher order finite element solutions. *Frontiers in Physics*, 10, 1079641. doi: 10.3389/ fphy.2022.1079641

[10] Lakahal, Y., & Laidoudi, H. (2025). Unraveling flow and thermal behavior of non-Newtonian fluids in triangular chambers: A computational study. *Heat Transfer*, 54(6), 4139–4152. doi: 10.1002/htj.23404

[11] Sharma, D.K., & Rana, B.K. (2025). Role of power-law fluids on mixed convection flows around revolving sphere. *Sādhanā*, 50(4), 257. doi: 10.1007/s12046-025-02896-7

[12] Thohura, S., Molla, M., Sarker, Md.M., Sarker, M.M.A., & Paul, M.C. (2021). Study of mixed convection flow of power-law fluids in a skewed lid-driven cavity. *Heat Transfer*, 50(6), 6328–6357. doi: 10.1002/htj.22174

[13] Hussain, S., Jamal, M., & Geridonmez, B.P. (2021). Impact of power law fluid and magnetic field on double diffusive mixed convection in staggered porous cavity considering Dufour and Soret effects. *International Communications in Heat and Mass Transfer*, 121, 105075. doi: 10.1016/j.icheatmasstransfer.2020. 105075

[14] Çolak, E., Ekici, Ö., & Öztop, H.F. (2021). Mixed convection in a lid-driven cavity with partially heated porous block. *International Communications in Heat and Mass Transfer*, 126, 105450. doi: 10.1016/j.icheatmasstransfer.2021.105450

[15] Kumar, S., Gangawane, K.M., & Oztop, H.F. (2021). A numerical study of mixed convection in a two-sided lid-driven tall cavity containing a heated triangular block for non-Newtonian power-law fluids. *Heat Transfer*, 50(5), 4806–4829. doi: 10.1002/htj. 22103

[16] Gangawane, K.M., & Oztop, H.F. (2020). Mixed convection in the semi-circular lid-driven cavity with heated curved wall subjugated to constant heat flux for non-Newtonian power-law fluids. *International Communications in Heat and Mass Transfer*, 114, 104563. doi: 10.1016/j.icheatmasstransfer.2020.104563

[17] Laidoudi, H. (2025). The effects of geometric shape and power-law index on the thermal activity and dynamic behavior of a complex fluid. *Emirates Journal for Engineering Research*, 30(1), 1. https://scholarworks.uaeu.ac.ae/ejer/vol30/iss1/1

[18] Vijayan, A., & Gangawane, K.M. (2021). Mixed convection in a tall lid-driven cavity with a triangular heat source for non-Newtonian power-law fluids. *Journal of Thermal Analysis and Calorimetry*, 146, 937–954. doi: 10.1007/s10973-020-10028-y

[19] Manchanda, M., & Gangawane, K.M. (2018). Mixed convection in a two-sided lid-driven cavity containing heated triangular block for non-Newtonian power-law fluids. *International Journal of Mechanical Sciences*, 144, 235–248. doi: 10.1016/j. ijmecsci.2018.06.005

[20] Gangawane, K.M., & Gupta, S. (2018). Mixed convection characteristics in rectangular enclosure containing heated elliptical block: Effect of direction of moving wall. *International Journal of Thermal Sciences*, 130, 100–115. doi: 10.1016/j.ijthermalsci. 2018.04.010

[21] Lakahal, Y., & Laidoudi, H. (2024). Flow and heat transfer of non-Newtonian fluids in confined triangular geometries: A computational approach. *Journal of the Serbian Society for Computational Mechanics*, 18(2), 110–127. doi: 10.24874/jsscm. 2024.18.02.07

[22] Aboud, E., Rashid, H., Jassim, H., Ahmed, S., Khafaji, S., Hamzah, H., & Ali, F. (2020). MHD effect on mixed convection of annulus circular enclosure filled with non-Newtonian nanofluid. *Heliyon*, 6(4), e03773. doi: 10.1016/j.heliyon.2020.e03773

[23] Bihiche, K., Lamsaadi, M., El hadoui, B., & Tizakast, Y. (2026). Double-diffusive natural convection of power-law fluids in an inclined square cavity with Soret effect. *Numerical Heat Transfer, Part A: Applications*, 87(1). doi: 10.1080/10407782.2025.2520816

[24] Barnoon, P., Toghraie, D., Dehkordi, R.B., & Abed, H. (2019). MHD mixed convection and entropy generation in a lid-driven cavity with rotating cylinders filled by a nanofluid using two-phase mixture model. *Journal of Magnetism and Magnetic Materials*, 483, 224–248. doi: 10.1016/j.jmmm.2019.03.108

[25] Selimefendigil, F., & Öztop, H.F. (2018). Mixed convection of nanofluids in a three-dimensional cavity with two adiabatic inner rotating cylinders. *International Journal of Heat and Mass Transfer*, 117, 331–343. doi: 10.1016/j.ijheatmasstransfer.2017.09.116

[26] Garmroodi, M.R.D., Ahmadpour, A., & Talati, F. (2019). MHD mixed convection of nanofluids in the presence of multiple rotating cylinders in different configurations: A two-phase numerical study. *International Journal of Mechanical Sciences*, 150, 247–264. doi: 10.1016/j.ijmecsci.2018.10.037

[27] Lakahal, Y., & Laidoudi, H. (2025). Buoyancy-driven flow and forced flow of complex fluid within a triangular chamber with a rotating body. *Acta Mechanica et Automatica*, 19(2), 224–240. doi: 10.2478/ama-2025-0027

[28] Hussain, S., & Öztop, H.F. (2021). Impact of inclined magnetic field and power-law fluid on double diffusive mixed convection in lid-driven curvilinear cavity. *International Communications in Heat and Mass Transfer*, 127, 105549. doi: 10.1016/j.icheatmasstransfer.2021.105549

[29] Nagarajan, S., & Ramachandran, S. (2025). Analysis of mixed convective-radiative heat transfer in a porous square cavity filled with various nanofluids. *Numerical Heat Transfer, Part A: Applications*, 86(1), 18–49. doi: 10.1080/10407782.2023.2257384

[30] Khalaf, A.F., Rashid, F.L., Basem, A., & Abbas, M.H. (2022). Numerical analysis in a lid-driven square cavity with hemispherical obstacle in the bottom. *Mathematical Modelling of Engineering Problems*, 9(6), 1639–1647. doi: 10.18280/mmep. 090625

[31] Rashid, F.L., Al-Gaheeshi, A.M.R., Alhwayzee, M., Ali, B., Shah, N.A., & Chung, J.D. (2023). Mixed convection in a horizontal channel–cavity arrangement with different heat source locations. *Mathematics*, 11(6), 1428. doi: 10.3390/ math11061428

[32] Rashid, F.L., Al-Gaheeshi, A.M.R., Rahman, M.H., & Basem, A. (2023). Mixed convection heat transfer in a channel-open cavity with two heat sources. *International Journal of Heat and Technology*, 41(1), 1–13. doi: 10.18280/ijht.410101

[33] Al-Gaheeshi, A.M.R., Rashid, F.L., Eleiwi, M.A., & Basem, A. (2023). Thermo-hydraulic analysis of mixed convection in a channel-square enclosure assembly with hemisphere source at the bottom. *International Journal of Heat and Technology*, 41(3), 551–562. doi: 10.18280/ijht.410307

[34] Ahmad, S., Ali, K., Sajid, T., Bashir, U., Rashid, F.L., Kumar, R., Ali, M.R., Hendy, A.S., & Darvesh, A. (2024). A novel vortex dynamics for micropolar fluid flow in a lid-driven cavity with magnetic field localization – A computational approach. *Ain Shams Engineering Journal*, 15(2), 102448. doi: 10.1016/j.asej.2023.102448

[35] Zhou, W., Yan, Y., Liu, X., Chen, H., & Liu, B. (2018). Lattice Boltzmann simulation of mixed convection of nanofluid with different heat sources in a double lid-driven cavity. *International Communications in Heat and Mass Transfer*, 97, 39–46. doi: 10.1016/j.icheatmasstransfer.2018.07.008

[36] Sindhu, T.N., Çolak, A.B., Lone, S.A., & Shafiq, A. (2023). Reliability study of generalized exponential distribution based on inverse power law using artificial neural network with Bayesian

regularization. *Quality and Reliability Engineering International*, 39(6), 2398–2421. doi: 10.1002/qre.3352

[37] Çolak, A.B., Sindhu, T.N., Lone, S.A., Shafiq, A., & Abushal, T.A. (2023). Reliability study of generalized Rayleigh distribution based on inverse power law using artificial neural network with Bayesian regularization. *Tribology International*, 185, 108544. doi: 10.1016/j.triboint.2023.108544

[38] Kuehn, T.H., & Goldstein, R.J. (1976). An experimental and theoretical study of natural convection in the annulus between horizontal concentric cylinders. *Journal of Fluid Mechanics*, 74(4), 695–719. doi: 10.1017/S0022112076002012

[39] Matin, M.H., & Khan, W.A. (2013). Laminar natural convection of non-Newtonian power-law fluids between concentric circular cylinders. *International Communications in Heat and Mass Transfer*, 43, 112–121. doi: 10.1016/j.icheatmasstransfer.2013.02. 006

[40] Matin, M.H., Pop, I., & Khanchezar, S. (2013). Natural convection of power-law fluid between two-square eccentric duct annuli. *Journal of Non-Newtonian Fluid Mechanics*, 197, 11–23. doi: 10.1016/j.jnnfm.2013.02.002

[41] Sheikholeslami, M. (2017). CuO–water nanofluid free convection in a porous cavity considering Darcy law. *The European Physical Journal Plus*, 132, 55. doi: 10.1140/epjp/i2017-11330-3

[42] Laidoudi, H., & Ameur, H. (2020). Investigation of the mixed convection of power-law fluids between two horizontal concentric cylinders: Effect of various operating conditions. *Thermal Science and Engineering Progress*, 20, 100731. doi: 10.1016/j.tsep.2020.100731